# Pauli limiting and metastability regions of superconducting graphene and intercalated graphite superconductors

F. D. R. Santos, A. M. Marques, and R. G. Dias
*Departamento de Física & I3N, Universidade de Aveiro, Campus Universitário de Santiago, 3810-193 Aveiro, Portugal*
(Received 23 September 2015; published 13 January 2016)

We present a study of metastability regions in the in-plane magnetic field versus temperature phase diagram of graphene and intercalated graphite superconductors. Due to the vanishing density of states, undoped graphene requires a finite BCS interaction $V_c$ to become superconducting (any finite doping drives this critical value to zero). Above $V_c$, superconducting graphene under in-plane magnetic field displays the conventional low temperature first-order transition (FOT) to the normal phase, but the width of the associated metastability region (normalized to the zero-temperature critical field) vanishes when doping goes to zero and the interaction approaches $V_c$. In the case of intercalated graphite superconductors, modeled as two-dimensional two-band superconductors (a graphene-like band and a metallic interlayer band), a critical graphene intraband interaction is required for the appearance of a second metastability region in the superconducting region of the phase diagram. The width of this metastability region also goes to zero as the graphene intraband interaction approaches, from above, its critical value and the metastability region vanishes at the zero-temperature supercooling field associated with the metallic interlayer band. Slightly above this critical value, the low-temperature FOT line bifurcates at an intermediate temperature into a FOT line and a second-order transition line.

DOI: 10.1103/PhysRevB.93.045412

## I. INTRODUCTION

In the past few years, several works have addressed electronic interactions in graphene, or more generally, in two-dimensional honeycomb lattices [1–7]. In the case of repulsive interactions, a transition between semimetallic and Mott insulating phases (that can display charge-density wave, spin-density wave, or quantum spin Hall orders) is observed as expected [1]. Recently, the possibility of superconducting phases driven by repulsive interactions in two-dimensional honeycomb lattices has also been addressed [2–5]. In particular, in the case of graphene, a chiral $d$-wave superconducting state has been proposed when doping forces the Fermi energy to the van Hove position [2]. For this particular doping value, the high density of states (DOS) and the Fermi surface nesting lead to a competition between superconducting and density wave instabilities, and according to renormalization-group calculations [2] a chiral $d$-wave superconducting phase is the most stable phase. More recently, the possibility of a $p + ip$ superconducting state in honeycomb lattices in the very strong repulsive Hubbard limit has also been proposed [3]. In this case, the Nagaoka ferromagnetic phase acts as the background where such a superconducting phase appears. On the other hand, the possibility of $s$-wave superconductivity in graphene driven by the usual effective attractive BCS interaction (which may reflect the conventional electron-phonon BCS mechanism) has also been addressed [6,7]. In this case, low critical temperature values are expected due to the vanishing DOS at the Fermi level. In our paper, we follow the latter works [6,7] and assume $s$-wave BCS superconductivity in graphene and graphite intercalation compounds (GICs).

Superconductivity is unlikely to be observed in isolated graphene due to its low dimensionality and resulting enhanced fluctuations, but also due to the semimetallic nature of graphene. In fact, using a simple BCS mean-field approach, one concludes that a critical pairing interaction is required for a superconducting phase to be present in graphene [6]. However, when doped, the Fermi energy of graphene shifts away from the Dirac point, where the density of states vanishes, and the finite DOS at the Fermi energy leads to a finite superconducting critical temperature for arbitrarily small attractive pairing potentials [6]. One should note that the absence of superconductivity in undoped graphene stated by the Mermin-Wagner theorem is in apparent contradiction with the mean-field approach. This theorem states that in materials with $D \leqslant 2$ (in which $D$ represents the dimensionality of a material), which is the case of graphene, long-range fluctuations can be created with little energy cost [8,9]. The appearance of such fluctuations decreases the chances of observing superconducting-like properties in strictly 2D materials. However, superconductivity in graphene is possible in tridimensional graphene-based structures.

A way of inducing superconductivity in graphene is by the proximity effect in S-G-S structures [10] (two superconducting metals connected to a graphene sheet). These systems are analogous to a two-band superconductor system with no intraband interactions in one of the bands, since the Josephson tunneling can be interpreted as an interband interaction [11–13]. Another way of inducing superconductivity in graphene is by intercalation of graphene sheets with metallic sheets. In GICs, superconductivity has been known to be present for almost half a century [14]. There has been a strong debate in the past few decades about whether GICs are one-band (due to the metallic interlayer band [15] or the graphene-like band [16]) or two-band superconductors (a graphene-like band and a metallic interlayer band) [17–24]. Recent high-resolution angle-resolved photoemission spectroscopy (ARPES) measurements, performed on $CaC_6$, present strong evidence supporting the scenario of both bands contributing to the superconducting phase [25].

The degree of anisotropy in GICs can be measured by the critical magnetic field anisotropy ratio $\Gamma_H = H_c^{\parallel}/H_c^{\perp}$ [26], where $H_c^{\parallel}$ ($H_c^{\perp}$) is the critical magnetic field when applied parallel (perpendicular) to the graphene sheets. The range of values for $\Gamma_H$ differs greatly from stage-1 to stage-2

 

GICs. Stage-1 compounds have been reported to have $\Gamma_H \sim 2$–$11$ [27,28], whereas in stage-2 compounds $\Gamma_H$ can have values that go up to 40 [27]. The very high anisotropy in stage-2 GICs suggests that they can be considered as quasi-2D materials. In these stage-2 superconducting GICs, and due to their reduced dimensionality, strongly attenuated orbital effects are expected when in-plane magnetic fields are applied. In such conditions, the orbital effect of the magnetic field becomes increasingly negligible as one moves away from the critical temperature $T_c$, with decreasing temperature, and the Zeeman effect becomes dominant. Near $T_c$, both Zeeman and orbital effects should be considered in a full description.

The in-plane magnetic field versus temperature phase diagram of quasi-2D one-band superconductors has been known for some time [29–31]. In particular, it has been shown that a curve of a first-order phase transition (FOT) and the respective metastability region (the region of coexistence of the homogeneous superconducting state and normal state local minima in the free energy) with increasing magnetic field are present at low temperatures, ending at a tricritical point around $T^\star \approx 0.56T_c$. For higher temperatures, $T > T^\star$, the transition becomes of second-order (SOT). In quasi-2D $n$-band superconductors with weak interband interactions, in addition to the above-mentioned first-order transition curve and metastability region, additional low-temperature FOT curves (more precisely, $n-1$ curves) and the corresponding metastability regions (limited below and above by the supercooling fields, $h_{sc}$, and by the superheating fields, $h_{sh}$, respectively) appear within the superconducting region of the phase diagram, each characterized by a large reduction in the superconducting gap of the band directly associated with the transition [32,33]. The additional low-temperature FOT and metastability regions present in the phase diagram are signaled by, respectively, additional crossings in the total free-energy difference between the superconducting and the normal phases, and reentrances in the band-gap solutions. Increasing the interband couplings has the effect of approaching the transitions within the superconducting region to the FOT to the normal phase, eventually making them disappear after the intersection for strong enough interband couplings.

In this work, we present a study of metastability regions in the phase diagram of superconducting graphene and intercalated graphite superconductors under in-plane magnetic fields using a weak-coupling BCS approach. We find that, due to the vanishing density of states at the Dirac point of graphene, the width of the metastability region associated with the low-temperature FOT to the normal phase (normalized to the zero-temperature critical field) shows a strong dependence on doping, vanishing at zero doping. In the case of intercalated graphite superconductors, modeled as 2D two-band superconductors, a critical pairing interaction is required for a second metastability region (associated primarily with the intraband pairing in the graphene-like band) to be present in the temperature versus in-plane magnetic field phase diagram. For intermediate values of the graphene intraband interaction above this critical value, a low-temperature FOT bifurcates at intermediate temperature into a FOT between superconducting phases and a SOT between the normal and the superconducting phase. These features are not exclusive to graphene-based superconductors and should also be observed in any quasi-2D superconductor with a semimetallic band.

## II. HAMILTONIAN AND GRAPHENE DOS

In this work, we use a simple weak-coupling description of $n$-band superconductors, adopting the Hamiltonian introduced by Sulh, Matthias, and Walker [34] with an additional Zeeman splitting term,

$$\mathscr{H} - \mu\mathscr{N} - \sigma h\mathscr{N} = \sum_{\mathbf{k}\sigma i} \xi_{\mathbf{k}\sigma i} c^\dagger_{\mathbf{k}\sigma i} c_{\mathbf{k}\sigma i} - \sum_{\mathbf{k}\mathbf{k}' ij} V^{ij}_{\mathbf{k}\mathbf{k}'} c^\dagger_{\mathbf{k}\uparrow j} c^\dagger_{-\mathbf{k}\downarrow j} c_{\mathbf{k}'\uparrow i} c_{-\mathbf{k}'\downarrow i}, \quad (1)$$

where $i,j = 1,2$ is the band index in the case of a two-band superconductor ($i,j = 1$ in the case of a one-band superconductor), $\mu$ is the chemical potential, $\sigma = \uparrow,\downarrow$ is the spin component along the in-plane magnetic field, $h = \mu_B H$, $\mu_B$ and $H$ are the Bohr magneton and the in-plane applied magnetic field, respectively, $\xi_{k\sigma i} = \varepsilon_{ki} - \mu - \sigma h$ is the kinetic energy term measured from $\mu$, and $V^{ij}_{\mathbf{k}\mathbf{k}'}$ gives the intraband ($i = j$) and interband ($i \neq j$) pairing interactions. It is worthwhile to note that a rigorous study for graphene-like band interactions above the critical interaction may require the introduction of the strong-coupling corrections, but the qualitative weak-coupling behavior should remain valid even taking into account these corrections [35].

Applying the mean-field approach to this Hamiltonian, and minimizing the respective free energy with respect to the superconducting gaps, one obtains an expression for the coupled superconducting gap equations [11,32], where $s$-wave symmetry is assumed,

$$\Delta_i = \sum_j V_{ij}\delta_j, \quad (2)$$

with

$$\delta_j = \delta_j(T,h,\Delta_j,N_j(\xi)) = \int_0^{\omega_D} d\xi\, \Delta_j \frac{N_j(\xi)}{2E_j}\left(\tanh\frac{E_j+h}{2k_BT} + \tanh\frac{E_j-h}{2k_BT}\right), \quad (3)$$

and where $E_j = \sqrt{\xi^2 + \Delta_j^2}$ is the quasiparticle excitation energy of the $j$ band, $\omega_D$ is the usual frequency cutoff, $N_j(\xi)$ is the DOS of the $j$ band, $T$ is the temperature, and $k_B$ is the Boltzmann constant. In the case of a one-band superconductor, one has a single gap equation ($i = 1$ and $j = 1$). In the weak-coupling BCS approximation, the physics is dominated by the cutoff induced by temperature or magnetic fields, and $\omega_D$ plays an irrelevant role apart from a renormalization factor, and we can set $\omega_D = D$.

The total free-energy difference between the superconducting and the normal phase, derived in detail in [33], is given by

$$F_s - F_n = k_BT \sum_{k\sigma i} \ln\frac{1 - f\left(E^\sigma_{ki}\right)}{1 - f\left(\left|\xi^\sigma_{ki}\right|\right)} + 2\sum_{|k|>k_f}(\xi_{ki} - E_{ki}) + \sum_i \delta_i\Delta_i, \quad (4)$$

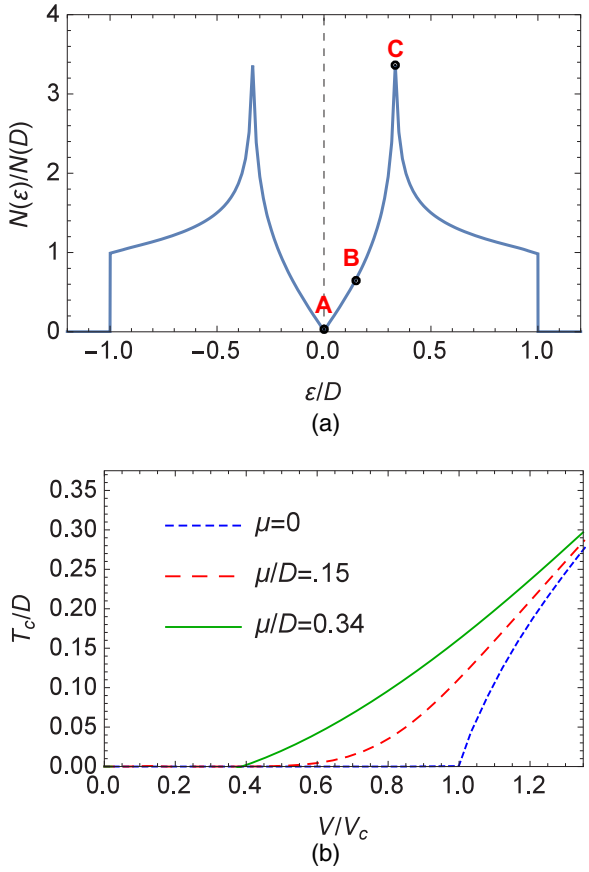


FIG. 1. (a) DOS of graphene (normalized to its value at the half-bandwidth $D$) as a function of energy (normalized to $D$). (b) Critical temperature at zero magnetic field (normalized to $D$) as a function of the BCS pairing interaction (normalized to the critical interaction value $V_c$) for several values of doping, indicated by points $A$, $B$, and $C$ in the top plot.

where $E_{ki} = E^{\sigma}_{ki} + \sigma h$ is the quasiparticle excitation energy in the absence of any applied magnetic field, and $|\xi^{\sigma}_{ki}| = |\xi_{ki}| - \sigma h$ is the kinetic energy of a normal electron in band $i$, in state $k$, with spin $\sigma$, measured from the Fermi energy.

Given that only a small strip of electron states around the Fermi energy participates in the superconducting phase in the weak-coupling limit of the BCS theory, it is usual to consider a constant DOS in this region [$N(\xi) = N(0) = N$]. This approximation is no longer valid in graphene bands since the Fermi energy coincides with the Dirac point, where the DOS is zero, as shown in Fig. 1(a). The DOS plot of Fig. 1(a) was taken by considering the standard tight-binding Hamiltonian with in-plane nearest-neighbor hopping in the graphene honeycomb lattice [36]. The energy is normalized to the half-bandwidth $D = 3t$, where $t$ is the hopping energy constant of the honeycomb lattice.

## III. SUPERCONDUCTIVITY IN GRAPHENE

In the case of a single graphene band, we can determine from Eqs. (2) and (3) if a superconducting phase will be present given different values of pairing strength $V$ and doping $\mu$. If there is a superconducting phase, one should find a positive finite $T_c$ when $\Delta$ is set to zero. The results for three different electron doping levels, $\mu/D = 0$, $\mu/D = 0.15$, and $\mu/D = 0.34$, are shown in Fig. 1(b) (the results are the same if we choose to hole dope the graphene band). In undoped graphene, there is a critical value of the pairing strength, which we call $V_c$, above which the system is a superconductor [6,7]. As soon as we start doping, this critical interaction goes to zero, that is, for arbitrarily small $V$, $T_c$ is *nonzero* (but very small). For a fixed $V$, $T_c$ increases with $\mu$ up to the van Hove singularity energy [point $C$ in Fig. 1(a)], reflecting the BCS dependence of $T_c$ on the DOS around the Fermi energy. The curves in Fig. 1(b) share the same asymptotic behavior for $T_c \sim \Delta \gg \mu$.

The distinct DOS profile of graphene shown in Fig. 1(a), and in particular its semimetallic nature, is responsible for new features in the superconducting phase when an in-plane magnetic field is applied. The in-plane magnetic field versus temperature superconducting phase diagram of a single graphene sheet for $V = 1.03V_c$, where $V_c/D = 0.0058$, and several values of chemical potential, $\mu/D = 0$, $\mu/D = 0.15$, and $\mu/D = 0.34$ [points $A$, $B$, and $C$ in Fig. 1(a), respectively], are shown in Fig. 2(a). The general behavior of the phase diagram for the three cases follows closely the one described in the Introduction for typical one-band superconductors, namely having a FOT curve between superconducting and normal phase at low temperatures, with its associated metastability region and becoming a SOT curve above some tricritical temperature in the high-temperature region of the phase diagram [29,30]. There are, however, two important differences: the area of the normalized metastability region is not constant, as in typical weak coupling one-band superconductors [30]. This area becomes very small (it vanishes as $V$ goes, from above, to the critical interaction $V_c$) as doping goes to zero (that is, as the Fermi level approaches the Dirac point). Furthermore, there is not a universal value for the tricritical temperature, which can take values $T^{\star} < 0.56T_{c0}$, becoming smaller as $\mu \to 0$ [see Fig. 2(a) (I)]. In the undoped case of Fig. 2(a) (I), the region of metastability is very narrow and becomes much larger for the intermediate doping level, at Fig. 2(a) (II), achieving its maximum width when the doping is such that the Fermi energy coincides with the van Hove singularity, as in Fig. 2(a) (III), as predicted in [31]. The evolution of the zero-temperature width of the metastability region with doping becomes more clear in Fig. 2(b), where it is shown for three values of the pairing strength: $V = 0.78V_c$, $V = V_c$, and $V = 1.03V_c$. For the latter two cases, the zero-temperature width of the metastability region increases sharply at low doping and nearly saturates at intermediate dopings, reaching its maximum value when the doping factor shifts the Fermi level to the van Hove singularity, as can be seen in Fig. 2(b). For $V = V_c$, the width is zero for $\mu = 0$. In contrast, for $V = 1.03V_c$, the width is finite everywhere, even when $\mu = 0$. In the first case, i.e., for $V = 0.78V_c$ the metastability region curve has a similar behavior to the other two cases, however in this case the low $\mu$ behavior implies very low critical fields outside the numerical range of our study.

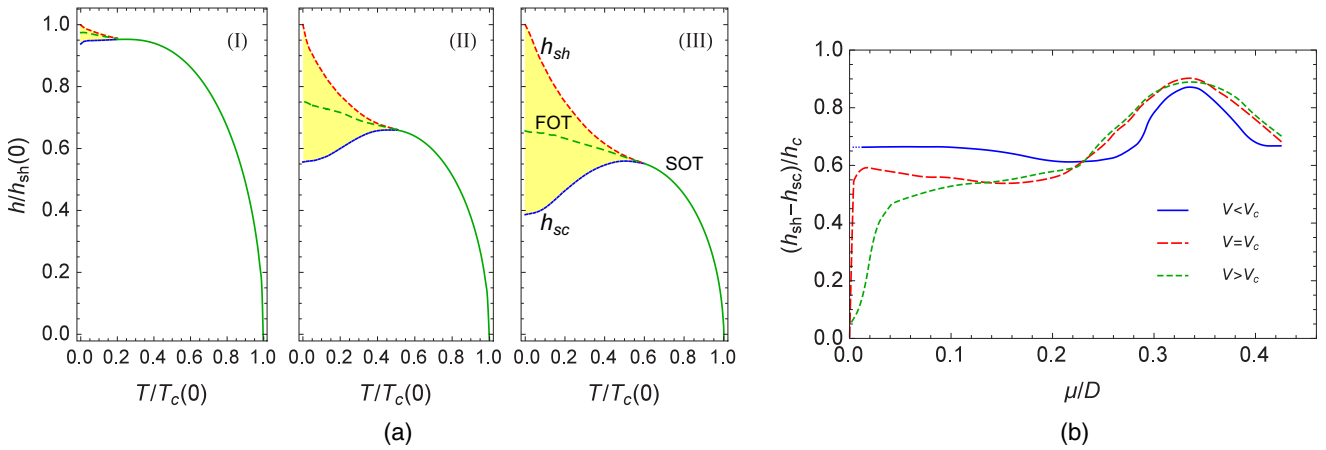


FIG. 2. (a) In-plane magnetic field [normalized to the zero-temperature superheating field $h_{sh}(0)$] vs temperature [normalized to the zero-field critical temperature $T_c(0)$] phase diagram of graphene, for (I) $\mu/D = 0$, (II) $\mu/D = 0.15$, and (III) $\mu/D = 0.34$ for $V = 1.03V_c$. For $\mu = 0$, the metastability region (yellow shaded area) is very narrow, and with doping, from (I) to (III), its normalized width increases as the Fermi energy is shifted away from the Dirac point. (b) Zero-temperature width (normalized to the zero-temperature critical field) behavior of the metastability region with doping, for $V = 0.78V_c$, $V = V_c$, and $V = 1.03V_c$. The width is zero at $\mu = 0$ for $V = V_c$, but it increases sharply for small $\mu$. For $V = 0.78V_c$, low $\mu$ implies very small critical fields and temperatures, these values being out of the numerical range of our study and consequently not shown in the figure.

## IV. INTERCALATED GRAPHITE UNDER IN-PLANE MAGNETIC FIELDS

As we mentioned in the Introduction, superconductivity was found in GICs several decades ago. Since these compounds have a graphene-like band in the band structure, it is natural to ask how much of the behavior shown in the previous section can be observed in these compounds. A simple approach one can use to address superconductivity in highly anisotropic GICs, while still preserving the essential characteristics of real materials, is a two-band model in which one of the bands is treated as a graphene-like band and the other as a generic 2D metallic band. Highly anisotropic GICs are primarily stage-2, which, by definition, are composed of intercalated graphene bilayers. The DOS profile of graphene bilayers is different from that of a single graphene sheet of Fig. 1(a) [37] due to the splitting of the van Hove singularity and to a slight modification around the Fermi energy. Assuming that the energy scale of these features is much smaller than the GIC superconducting gaps, these differences can be neglected, i.e., one can assume the DOS shown in Fig. 1(a) even in the case of stage-2 GICs.

In what follows, the metallic interlayer and graphene-like bands are labeled bands 1 and 2, respectively. The values considered for the matrix of potentials, necessary to find the superconducting gaps via Eq. (2), are

$$\begin{pmatrix} V_{11} & V_{12} \\ V_{21} & V_{22} \end{pmatrix} N_1(0) \rightarrow \begin{pmatrix} 0.2 & 0.008 \\ 0.008 & V_{22} \end{pmatrix}, \tag{5}$$

where $V_{11}$ is the intraband potential of the metallic interlayer band, $V_{22}$ is the intraband potential of the graphene-like band, $V_{12} = V_{21}$ is the interband potential that couples the two bands, and $N_1(0)$ is the density of states of the metallic band at the Fermi energy. The relation between the density of states of the graphene-like band and the metallic interlayer band is set by the condition $N_2(D) = 1.24N_1(0)$, where $N_2(D)$ is the density of states of the graphene-like band at the band edge. To simplify the notation, we will drop the $N_1(0)$ term when indicating interaction values.

The existence of a finite interband coupling implies that the graphene-like band becomes superconducting (has a finite superconducting gap) for any value of $V_{22}$, even when the Fermi energy coincides with the Dirac point energy of the graphene-like band. Thus, there is not a critical value of the graphene-like intraband coupling as in the case of the isolated one-band graphene superconductor. This reflects the Josephson tunneling of Cooper pairs from the metallic band (this is similar to the effect of an external magnetic field in a paramagnetic system) and it is also the justification for the existence of a single critical superconducting temperature in the case a two-band superconductor with two metallic bands. However, a new critical intraband coupling $V_{c2}$ for the graphene-like band can be defined, associated with the appearance of a second metastability region in the superconducting phase of the in-plane magnetic field versus temperature phase diagram. This fact can be understood by the fact that the second metastability region reflects the existence of intrinsic pairing in the graphene-like band, and this requires a finite intraband interaction. This second metastability region is always present in a two-band superconductor when both bands have constant DOS at the Fermi energy and the interband coupling is weak. In the case studied here, for small $V_{22}$, the second metastability region is not present, reflecting precisely the absence of intrinsic superconductivity in an isolated (weak coupled) graphene layer in the weak interband coupling limit. Since $V_{c2}$ depends on $V_{11}$, $V_{22}$, and $V_{12}$, we do not normalize these interactions to a critical interaction. Instead, we choose to normalize the interactions to $N_1(0)$, as stated above.

As before, by changing the doping factor $\mu$, we are shifting the Fermi level in the graphene-like band, therefore changing the profile of $N_2(\xi)$ in Eq. (3), whereas in the case of the metallic band, as usual in BCS theory, we consider a constant DOS, $N_1(\xi) = N_1(0)$. First, we study our two-band model for $\mu/D = 0$, that is, the Fermi level coincides with the Dirac

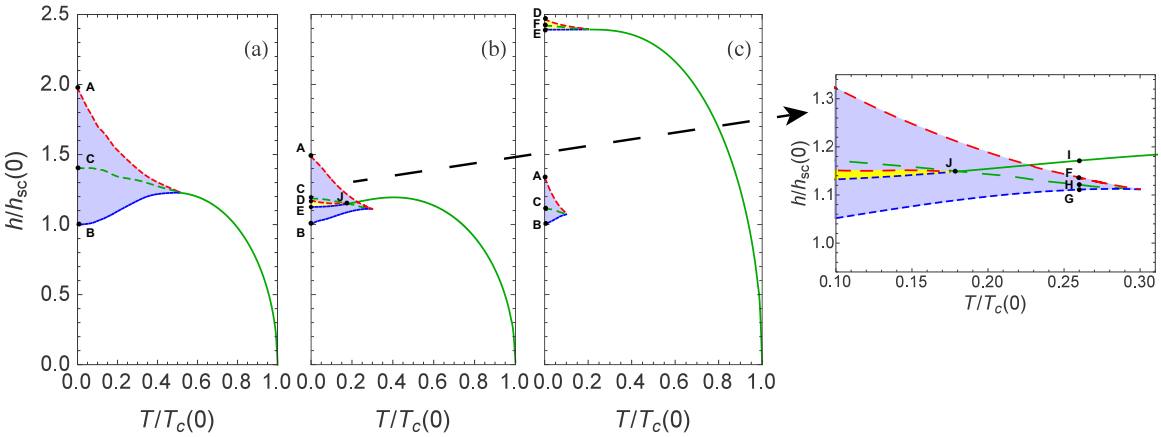


FIG. 3. In-plane magnetic field [normalized to the zero-temperature supercooling field $h_{sc}(0)$] vs temperature [normalized to the zero-field critical temperature $T_c(0)$] phase diagram of intercalated graphite (using a two-band BCS description) for (a) $V_{22} = 0.18$, (b) $V_{22} = 0.24$, and (c) $V_{22} = 0.26$. The metastability region associated primarily with intraband pairing in the metallic (graphene) band is shown in the blue (yellow) shaded area. From (a) to (c) the phase diagram changes from that of a typical one-band to that of a typical two-band superconductor phase diagram. In the intermediate case (b), unusual behavior occurs: in the zoomed plot of (b) one can see, at a temperature $T \approx 0.175T_c$, that the FOT (dashed green curve $C$-$J$) splits into an upper SOT (solid green curve $J$-$I$) and an additional lower FOT (dashed green curve $J$-$H$). The labeled points correspond to those in Figs. 4 and 5(a).

point energy of the graphene-like band DOS for three different cases: $V_{22} = 0.18$, $V_{22} = 0.24$, and $V_{22} = 0.26$, these values being, respectively, smaller, slightly larger, and larger than $V_{c2}$, where $V_{c2}/D = 0.006$. The in-plane magnetic field versus temperature phase diagram for these three cases is shown in Fig. 3, and the corresponding zero-temperature gap solutions and the total free-energy difference between superconducting and normal phase as functions of the magnetic field is shown in Figs. 4(a), 4(e), and 4(i), respectively.

In the case of $V_{22} = 0.18$, the phase diagram obtained, Fig. 3(a), has the same behavior as that of a single-band BCS superconductor [only one metastability zone (blue shaded area) and one FOT (green curve, which starts at the point $C$) are present in the phase diagram]. This behavior can be confirmed from the zero-temperature band-gap solutions shown in Fig. 4(a), where one may observe, for each band, the presence of only one reentrance in the band-gap solutions and no crossing in the free-energy difference between superconducting and normal phase. This result implies that $V_{22} < V_{c2}$. Even though the graphene-like band is also superconducting (because $\Delta_2$ is finite), since $\Delta_2$ is much smaller than $\Delta_1$, we may say that the superconductor behavior of this system is due to intrinsic superconducting correlations of the metallic interlayer band.

When one increases the graphene-like band intraband interaction to a value a little higher than $V_{c2}$ (i.e., the case of $V_{22} = 0.24$), the influence of the graphene-like band is no longer negligible, and even though there is no additional low-temperature transition between superconducting phases, an extra metastability region, associated with the graphene-like band, appears (small yellow shaded region delimited by points $D$, $E$, and $J$ in Fig. 3). This behavior can be checked in Fig. 4(e), where one observes that there is no crossing in the free energy, but one observes the presence of two reentrances (points $A$-$B$ and $D$-$E$) in the zero-temperature band-gap solutions. Since an additional FOT should be present in the phase diagram for it to be considered one of a typical two-band superconductor, for $V_{22} \gtrsim V_{c2}$ the system can be seen as an intermediate case between a one-band and a two-band superconductor. Furthermore, for temperatures in the $0.175T_c < T < 0.3T_c$ range, the system exhibits a rather unusual feature. One may see in the zoomed plot of Fig. 3 that the low-temperature FOT (dashed green curve that starts at point $C$) splits, at an intermediate temperature (point $J$), into an upper SOT (solid green curve $J$-$I$) between the normal and the superconducting phase and into a lower FOT (dashed green curve $J$-$H$) that reflects a transition between superconducting phases. This is understood as a consequence of the crossing of the metastability regions associated with the graphene-like band and the metallic band as the graphene-like intraband pairing interaction is increased. The bifurcation occurs because the metastability region of the graphene-like band is much narrower than that of the metallic band. These two transitions are not the continuation of the low-temperature FOT. In fact, in this case the SOT is the continuation of an additional supercooling field at low temperature (dashed blue curve that goes from point $E$ to point $J$). We can confirm the splitting of the FOT by analyzing the band-gap solutions and the free energy, for $T = 0.26T_c$, shown in Fig. 5(a). On the one hand, the band-gap solution curves go smoothly to zero (point $I$) at large fields (i.e., a SOT occurs), but on the other hand, the crossing in the free energy (point $H$) occurs before the SOT between the superconductor and the normal phase (i.e., an additional FOT occurs).

It is expected that by increasing $V_{22}$ even more, the superconducting phase diagram will finally change into a typical two-band superconductor phase diagram. Indeed, for $V_{22} = 0.26$, two FOTs (dashed green curves that start at $C$ and $F$) and the two respective metastability regions (points $A$-$B$ and $D$-$E$, respectively) are present at low temperature in the phase diagram, Fig. 3(c). One of them corresponds to the superconducting to normal transition (yellow shaded area) and is due to the graphene-like band, and the other (blue shaded area), which is due to the metallic interlayer band, corresponds to an FOT between different superconducting phases. The additional low-temperature FOT between superconducting

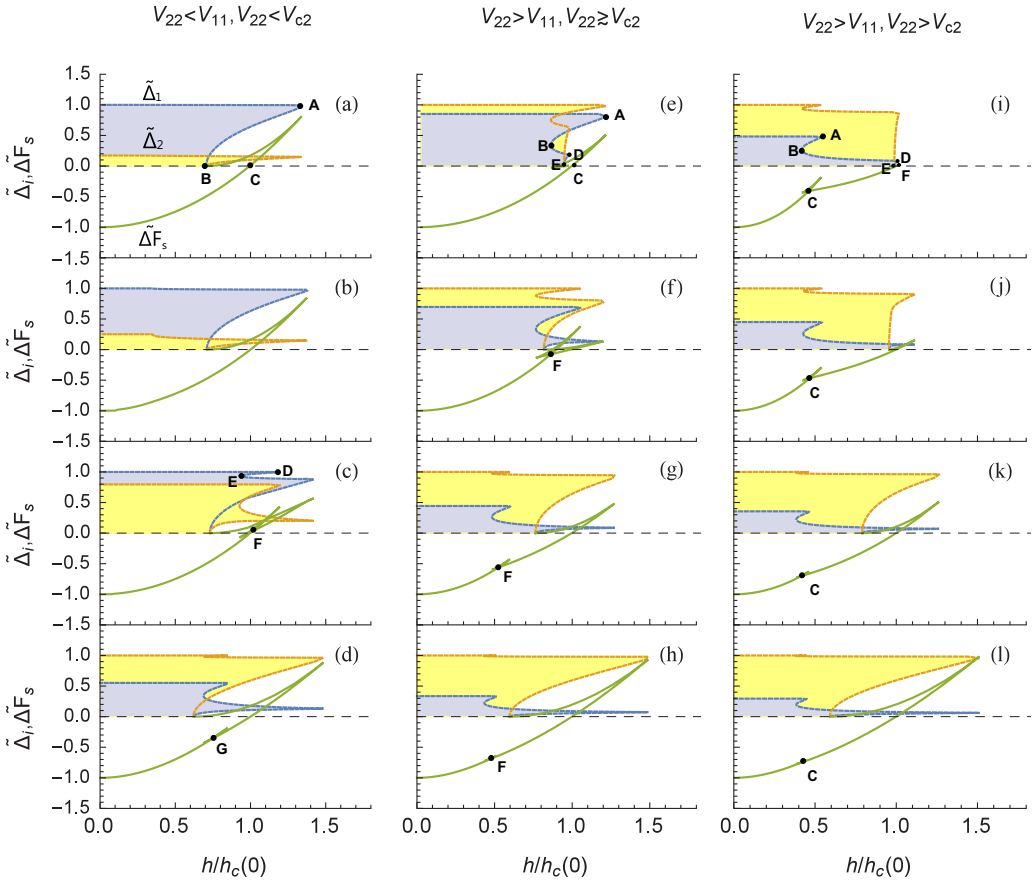


FIG. 4. Zero-temperature solutions of the coupled gap equations (normalized to the maximum gap) and the total free-energy difference between the superconducting and the normal phases (normalized to its zero-field value) of intercalated graphite. The in-plane magnetic fields are normalized to the zero-temperature critical field $h_c(0)$. The first, second, and third columns correspond to $V_{22} = 0.18$ (a)–(d), $V_{22} = 0.24$ (e)–(h), and $V_{22} = 0.26$ (i)–(l), respectively, and the first to the fourth rows correspond to $\mu = 0$, $\mu/D = 0.05$, $\mu/D = 0.15$, and $\mu/D = 0.34$, respectively. For $V_{22} = 0.18$, with increasing doping, the phase diagram changes from that of a typical one-band [(a)] to that of a two-band superconductor [(d)], as an additional reentrance (curve $D$-$E$) and FOT (point G) appear in the superconducting phase diagram. In (e), even though one identifies two reentrances, an additional FOT between superconducting phases only appears when we dope the graphene-like band (point $F$). In (i), the phase diagram shows typical two-band superconductor behavior.

phases can be observed in the zero-temperature band-gap solutions, Fig. 4(i), where the crossing in the free energy, at point $C$, occurs before it changes its sign at point $F$.

The profile change of the phase diagram from that of a one-band to that of a two-band superconductor due to the increase of $V_{22}$ is shown in detail in Figs. 6(a)–6(e) for,

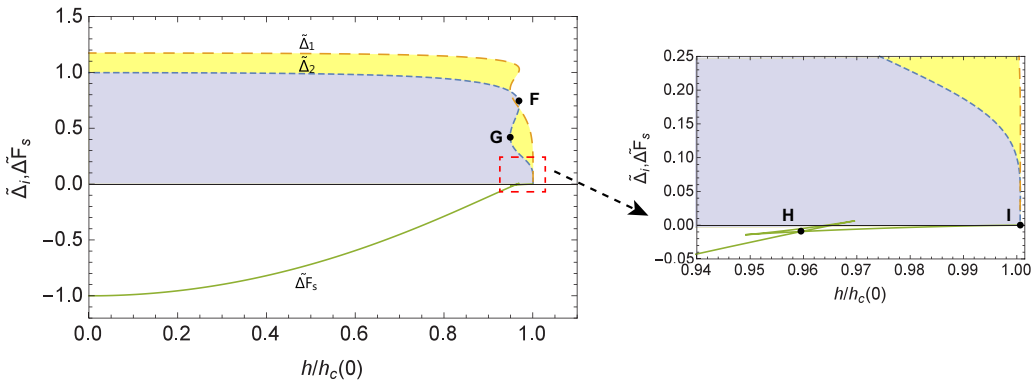


FIG. 5. (a) Solutions of the coupled gap equations and the total free-energy difference between the superconducting and the normal phases of a two-band intercalated graphite superconductor at $T = 0.26T_c$ for $V_{22} = 0.26$ and a zoomed region showing a crossing in the free energy before the SOT to the normal phase. The labeled points correspond to those in Fig. 3.

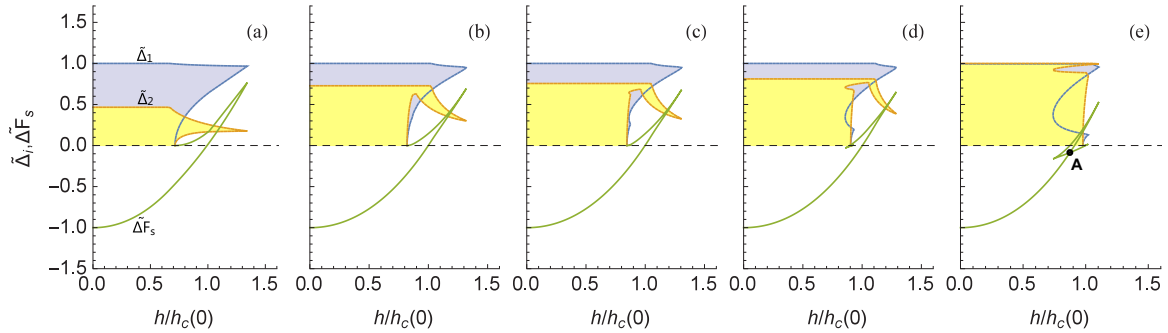


FIG. 6. Zero-temperature gap solutions for intercalated graphite for (a) $V_{22} = 0.26$, (b) $V_{22} = 0.262$, (c) $V_{22} = 0.266$, (d) $V_{22} = 0.268$, and (e) $V_{22} = 0.28$. Other parameters are as follows: $\mu/D = 0$, $V_{11} = 0.28$, and $V_{12} = 0.008$. In (c), a small additional reentrance arises in the gap solution curves at the supercooling field associated with the metallic interlayer band. This reentrance widens as we increase $V_{22}$, and an additional FOT between superconducting phases occurs in (e) at point $A$.

respectively, $V_{22} = 0.26$, $V_{22} = 0.262$, $V_{22} = 0.266$, $V_{22} = 0.268$, and $V_{22} = 0.28$, and fixed parameters $V_{11} = 0.028$ and $V_{12} = 0.008$. At $V_{22} = 0.266$ [Fig. 6(c)], a small reentrance appears in both gap solution curves and grows as we increase $V_{22}$. An additional FOT between superconducting phases occurs when $V_{22} = 0.28$ [Fig. 6(e), point $A$]. An interesting feature of these plots is that the additional reentrance arises at the supercooling field associated with the metallic interlayer band. This can be understood as a natural consequence of going from the gap curves of a one-band superconductor [which have only one reentrance at zero temperature; see Figs. 4(a) and 4(b)] to the typical behavior of a two-band superconductor where the superconducting gaps show two reentrances at zero temperature [see Figs. 4(c)–4(e)]. Furthermore, using a different $V_{11}$ from the case of Fig. 4, we show that $V_{c2}$ depends on $V_{11}$. Comparing the values of $V_{11}$ and $V_{c2}$ between the case of Fig. 4 ($V_{11} = 0.2$, $V_{c2} = 0.24$) with that of Fig. 6 ($V_{11} = 0.28$, $V_{c2} = 0.266$), one concludes that an increase of $V_{11}$ leads to an increase of $V_{c2}$.

We conclude that increasing $V_{22}$ from $V_{22} < V_{c2}$ to $V_{22} > V_{c2}$ causes the system to behave as a typical two-band superconductor. Let us now consider what happens if we fix $V_{22}$ and instead dope the graphene layer. The zero-temperature gap solutions for the $V_{22} = 0.18$, $V_{22} = 0.24$, and $V_{22} = 0.26$ cases for small doping, $\mu/D = 0.05$, intermediate doping, $\mu/D = 0.15$, and large doping, $\mu/D = 0.34$, are shown in Figs. 4(b)–4(d), 4(f)–4(h), and 4(j)–4(l).

In the case of the left column [Figs. 4(a)–4(d)], increasing $\mu$ allows for the appearance of the additional reentrance [see Fig. 4(c), points $D$ and $E$]. However, the crossing in the free-energy difference between the superconducting and the normal phase, at point $F$, occurs after it changes its sign. For large $\mu$, Fig. 4(d), the system finally shows the additional transition between superconducting phases since the crossing in the free-energy difference between the superconducting and the normal phase, at point $G$, occurs before it changes its sign. Thus, in this case, the phase diagram behaves like that of a typical two-band superconductor. In the case of the middle column [Figs. 4(e)–4(h)], due to the fact that $V_{22} \gtrsim V_{c2}$, a small $\mu$ is enough to obtain a phase diagram such as that of a two-band superconductor since one observes the appearance of the additional FOT [Fig. 4(f), point $F$]. In the case of the right column [Figs. 4(i)–4(l)], one observes the increase of the metastability region width, associated with the graphene-like band, with increasing doping [Figs. 4(j)–4(l)]. In general, doping the graphene-like band causes a change in the GICs phase diagram from a one-band superconductor-like phase diagram to a two-band superconductor-like phase diagram. Furthermore, when the metastability region associated with the graphene-like band is present, its normalized width increases with doping, a feature that is expected when taking into account what we concluded in the previous section.

## V. CONCLUSION

In conclusion, we studied metastability regions in the phase diagram of superconducting graphene and intercalated graphite superconductors under an in-plane magnetic field in both doped and undoped cases using a simple BCS multiband approach. In the case of a single undoped graphene band, a critical intraband interaction is required for a superconducting phase to be present in undoped graphene, but this critical intraband interaction vanishes for any finite doping. We showed that the introduction of doping in a graphene band also affects the behavior of the metastability region of the in-plane magnetic field versus temperature phase diagram. The normalized area of the metastability region and the tricritical temperature value become smaller as doping goes to zero, in contrast with the case of a doped metallic band.

We have also studied the in-plane magnetic field versus temperature phase diagram of an intercalated graphite superconductor, modeled as a two-dimensional two-band superconductor with one graphene-like band and a metallic interlayer band. In this case, finite interband pairing interactions imply the existence of a superconducting phase with finite superconducting gaps in both bands, that is, there is no critical intraband interaction for the graphene-like band. However, we found a new intraband critical interaction for the graphene-like band associated with the appearance of a second metastability region in the phase diagram. The phase diagrams obtained for a smaller and larger intraband interaction (of the graphene-like band) than the critical interaction are those of a typical one-band and two-band superconductor, respectively. When the intraband interaction of the graphene-like band is just slightly larger than this critical interaction, new features are observed in the phase diagram, such as the

absence of the low-temperature first-order transition between superconducting phases and at an intermediate temperature, and the bifurcation of the low-temperature first-order transition curve into a first-order transition between superconducting phases and a second-order transition between the normal and the superconducting phase. The second metastability region arises with increasing graphene-like band intraband interaction, emerging at the zero-temperature supercooling field associated with the metallic interlayer band.

The phase diagrams of Fig. 3 provide a background against which future experimental data concerning superconductivity on GICs should be interpreted. If future measurements of superconducting in-plane critical fields in GICs find two low-temperature first-order transitions, this would imply that both the graphene-like band and the metallic interlayer band participate in the superconducting phase [17–24]. On the other hand, the presence of only one low-temperature first-order transition would not, by itself, conclusively disprove a two-band description in favor of a one-band description [15,16] since, as we showed in Fig. 3(a), both bands can be superconducting even if the in-plane magnetic field versus temperature phase diagram is that of a typical one-band superconductor.

## ACKNOWLEDGMENTS

This work is funded by the FEDER funds through the COMPETE 2020 Programme and National Funds through FCT–Portuguese Foundation for Science and Technology under the project UID/CTM/50025/2013. A.M.M. acknowledges the financial support from the (FCT-Portuguese Foundation for Science and Technology through Grant No. PD/BD/108663/2015.

[1] S. Raghu, X.-L. Qi, C. Honerkamp, and S.-C. Zhang, Topological Mott Insulators, Phys. Rev. Lett. **100**, 156401 (2008).

[2] R. Nandkishore, L. S. Levitov, and A. V. Chubukov, Chiral superconductivity from repulsive interactions in doped graphene, Nat. Phys. **8**, 158 (2012).

[3] Z.-C. Gu, H.-C. Jiang, and G. Baskaran, Emergence of $p+ip$ superconductivity in 2D strongly correlated Dirac fermions, arXiv:1408.6820.

[4] T. Ma, F. Yang, H. Yao, and H.-Q. Lin, Possible triplet $p+ip$ superconductivity in graphene at low filling, Phys. Rev. B **90**, 245114 (2014).

[5] X. Chen, Y. Yao, H. Yao, F. Yang, and J. Ni, Topological $p+ip$ superconductivity in doped graphene-like single-sheet materials $BC_3$, Phys. Rev. B **92**, 174503 (2015).

[6] N. B. Kopnin and E. B. Sonin, BCS Superconductivity of Dirac Electrons in Graphene Layers, Phys. Rev. Lett. **100**, 246808 (2008).

[7] B. Uchoa and A. H. Castro Neto, Superconducting States of Pure and Doped Graphene, Phys. Rev. Lett. **98**, 146801 (2007).

[8] N. D. Mermin, Absence of ordering in certain classical systems, J. Math. Phys. **8**, 1061 (1967).

[9] N. D. Mermin and H. Wagner, Absence of Ferromagnetism or Antiferromagnetism in One- or Two-Dimensional Isotropic Heisenberg Models, Phys. Rev. Lett. **17**, 1133 (1966).

[10] H. le Sueur, P. Joyez, H. Pothier, C. Urbina, and D. Esteve, Phase Controlled Superconducting Proximity Effect Probed by Tunneling Spectroscopy, Phys. Rev. Lett. **100**, 197002 (2008).

[11] A. J. Leggett, Number-phase fluctuations in two-band superconductors, Progr. Theor. Phys. **36**, 901 (1966).

[12] D. F. Agterberg, E. Demler, and B. Janko, Josephson effects between multigap and single-gap superconductors, Phys. Rev. B **66**, 214507 (2002).

[13] P. J. W. Moll, X. Zhu, P. Cheng, H.-H. Wen, and B. Batlogg, Intrinsic Josephson junctions in the iron-based multi-band superconductor $(V_2Sr_4O_6)$ $Fe_2As_2$, Nat. Phys. **10**, 644 (2014).

[14] N. B. Hannay, T. H. Geballe, B. T. Matthias, K. Andres, P. Schmidt, and D. MacNair, Superconductivity in Graphitic Compounds, Phys. Rev. Lett. **14**, 225 (1965).

[15] K. Sugawara, T. Sato, and T. Takahashi, Fermi-surface-dependent superconducting gap in $C_6Ca$, Nat. Phys. **5**, 40 (2009).

[16] T. Valla, J. Camacho, Z.-H. Pan, A. V. Fedorov, A. C. Walters, C. A. Howard, and M. Ellerby, Anisotropic Electron-Phonon Coupling and Dynamical Nesting on the Graphene Sheets in Superconducting $C_6Ca$ Using Angle-Resolved Photoemission Spectroscopy, Phys. Rev. Lett. **102**, 107007 (2009).

[17] G. Profeta, M. Calandra, and F. Mauri, Phonon-mediated superconductivity in graphene by lithium deposition, Nat. Phys. **8**, 131 (2012).

[18] M. Calandra and F. Mauri, Theoretical Explanation of Superconductivity in $C_6Ca$, Phys. Rev. Lett. **95**, 237002 (2005).

[19] A. Sanna, G. Profeta, A. Floris, A. Marini, E. K. U. Gross, and S. Massidda, Anisotropic gap of superconducting $CaC_6$: A first-principles density functional calculation, Phys. Rev. B **75**, 020511 (2007).

[20] L. Boeri, G. B. Bachelet, M. Giantomassi, and O. K. Andersen, Electron-phonon interaction in graphite intercalation compounds, Phys. Rev. B **76**, 064510 (2007).

[21] J. S. Kim, R. K. Kremer, L. Boeri, and F. S. Razavi, Specific Heat of the Ca-Intercalated Graphite Superconductor $CaC_6$, Phys. Rev. Lett. **96**, 217002 (2006).

[22] G. Lamura, M. Aurino, G. Cifariello, E. Di Gennaro, A. Andreone, N. Emery, C. Hérold, J.-F. Marêché, and P. Lagrange, Experimental Evidence of $s$-Wave Superconductivity in Bulk $CaC_6$, Phys. Rev. Lett. **96**, 107008 (2006).

[23] N. Bergeal, V. Dubost, Y. Noat, W. Sacks, D. Roditchev, N. Emery, C. Hérold, J.-F. Marêché, P. Lagrange, and G. Loupias, Scanning Tunneling Spectroscopy on the Novel Superconductor $CaC_6$, Phys. Rev. Lett. **97**, 077003 (2006).

[24] R. S. Gonnelli, D. Daghero, D. Delaude, M. Tortello, G. A. Ummarino, V. A. Stepanov, J. S. Kim, R. K. Kremer, A. Sanna, G. Profeta, and S. Massidda, Evidence for Gap Anisotropy in $CaC_6$ from Directional Point-Contact Spectroscopy, Phys. Rev. Lett. **100**, 207004 (2008).

[25] S.-L. Yang, J. A. Sobota, C. A. Howard, C. J. Pickard, M. Hashimoto, D. H. Lu, S.-K. Mo, P. S. Kirchmann, and Z.-X. Shen, Superconducting graphene sheets in $CaC_6$ enabled by phonon-mediated interband interactions, Nat. Commun. **5** (2014).

[26] J. S. Kim, L. Boeri, J. R. O'Brien, F. S. Razavi, and R. K. Kremer, Superconductivity in Heavy Alkaline-Earth Intercalated Graphites, Phys. Rev. Lett. **99**, 027001 (2007).

[27] Y. Iye and S.-i. Tanuma, Superconductivity of graphite intercalation compounds with alkali-metal amalgams, Phys. Rev. B **25**, 4583 (1982).

[28] T. E. Weller, M. Ellerby, S. S. Saxena, R. P. Smith, and N. T. Skipper, Superconductivity in the intercalated graphite compounds $C_6Yb$ and $C_6Ca$, Nat. Phys. **1**, 39 (2005).

[29] K. Maki and T. Tsuneto, Pauli paramagnetism and superconducting state, Progr. Theor. Phys. **31**, 945 (1964).

[30] H. Shimahara, Fulde-Ferrell state in quasi-two-dimensional superconductors, Phys. Rev. B **50**, 12760 (1994).

[31] R. G. Dias and J. A. Silva, Huge metastability in high-$T_c$ superconductors induced by parallel magnetic field, Phys. Rev. B **67**, 092511 (2003).

[32] R. G. Dias, Zeeman splitting in multiple-band superconductors, Phys. Rev. B **72**, 012505 (2005).

[33] A. M. Marques, R. G. Dias, M. A. N. Araujo, and F. D. R. Santos, In-plane magnetic field vs. temperature phase diagram of a quasi-2D frustrated multiband superconductor, Supercond. Sci. Technol. **28**, 045021 (2015).

[34] H. Suhl, B. T. Matthias, and L. R. Walker, Bardeen-Cooper-Schrieffer Theory of Superconductivity in the Case of Overlapping Bands, Phys. Rev. Lett. **3**, 552 (1959).

[35] B. Uchoa, G. G. Cabrera, and A. H. Castro Neto, Nodal liquid and *s*-wave superconductivity in transition metal dichalcogenides, Phys. Rev. B **71**, 184509 (2005).

[36] A. H. Castro Neto, F. Guinea, N. M. R. Peres, K. S. Novoselov, and A. K. Geim, The electronic properties of graphene, Rev. Mod. Phys. **81**, 109 (2009).

[37] E. V. Castro, M. P. López-Sancho, and M. A. H. Vozmediano, Pinning and switching of magnetic moments in bilayer graphene, New J. Phys. **11**, 095017 (2009).